JACS
JOURNAL OF THE AMERICAN CHEMICAL SOCIETY
Article
pubs.acs.org/JACS

Bifunctional Porphyrin Catalysts for the Synthesis of Cyclic Carbonates from Epoxides and CO_2: Structural Optimization and Mechanistic Study

Tadashi Ema,*[,†] Yuki Miyazaki,[†] Junta Shimonishi,[†] Chihiro Maeda,[†] and Jun-ya Hasegawa*[,‡]

[†]Division of Chemistry and Biotechnology, Graduate School of Natural Science and Technology, Okayama University, Tsushima, Okayama 700-8530, Japan

[‡]Catalysis Research Center, Hokkaido University, Kita 21, Nishi 10, Kita-ku, Sapporo 001-0021, Japan

Supporting Information

ABSTRACT: We prepared bifunctional Mg^{II} porphyrin catalysts **1** for the solvent-free synthesis of cyclic carbonates from epoxides and CO_2. The activities of **1d**, **1h**, and **1i**, which have Br^-, Cl^-, and I^- counteranions, respectively, increased in the order **1i** < **1h** < **1d**. Catalysts **1d** and **1j**−**m**, which bear four tetraalkylammonium bromide groups with different alkyl chain lengths, showed comparable but slightly different activities. Based on the excellent catalyst **1d**, we synthesized Mg^{II} porphyrin **1o** with eight tetraalkylammonium bromide groups, which showed even higher catalytic activity (turnover number, 138,000; turnover frequency, 19,000 h^{-1}). The catalytic mechanism was studied by using **1d**. The yields were nearly constant at initial CO_2 pressures in the 1−6 MPa range, suggesting that CO_2 was not involved in the rate-determining step in this pressure range. No reaction proceeded in supercritical CO_2, probably because the epoxide (into which the catalyst dissolved) dissolved in and was diluted by the supercritical CO_2. Experiments with ^{18}O-labeled CO_2 and D-labeled epoxide suggested that the catalytic cycle involved initial nucleophilic attack of Br^- on the less hindered side of the epoxide to generate an oxyanion, which underwent CO_2 insertion to afford a CO_2 adduct; subsequent intramolecular ring closure formed the cyclic carbonate and regenerated the catalyst. Density functional theory calculations gave results consistent with the experimental results, revealing that the quaternary ammonium cation underwent conformational changes that stabilized various anionic species generated during the catalytic cycle. The high activity of **1d** and **1o** was due to the cooperative action of the Mg^{II} and Br^- and a conformational change (induced-fit) of the quaternary ammonium cation.

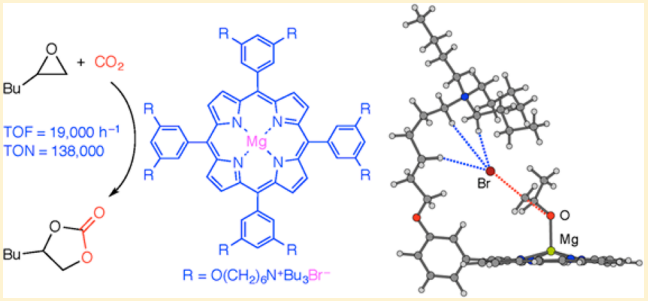

INTRODUCTION

Carbon dioxide (CO_2) is an inexpensive, nontoxic, and abundant carbon source for organic synthesis, and CO_2 has been converted into various valuable chemicals.[1−7] For example, cyclic carbonates, which are used as raw materials for polycarbonates, as electrolytes in lithium-ion secondary batteries, and as polar aprotic solvents, have been synthesized from CO_2 and epoxides with high atom efficiency. Various catalysts for this reaction have been developed,[4−7] including metal complexes (e.g., metal salen complexes and metalloporphyrins) and organocatalysts (e.g., quaternary ammonium salts and N-heterocyclic carbenes).

Among these catalysts, metalloporphyrins show relatively high catalytic activity.[6] Various metal ions can be incorporated into porphyrins, and the rigidity of the porphyrin framework permits control of the spatial arrangement of the functional groups attached to it.[8] Therefore, the catalytic activity of metalloporphyrins can be improved further by suitable functionalization. Bifunctional or trifunctional catalysts show high catalytic activity for various reactions owing to the cooperative effects of the catalytic functional groups.[3b,e,4d,Sb,h,9] In previous work, we designed and synthesized bifunctional porphyrin catalysts **1a**−**g** (Figure 1),[7] which showed high catalytic activity derived from the cooperative action of the nucleophilic halide anion (X^-) and the Lewis acid metal center (M). The organocatalytic moiety is attached to the *meta* position of the benzene ring in **1** to secure the coordination space of epoxide. The advantage of this catalytic motif is that strict adjustment of the spacer length is unnecessary because the X^- anion moves freely to attack the epoxide at an appropriate angle.[7] Metalloporphyrins **1c** and **1d** with quaternary tributylammonium bromide groups were more active than **1a** and **1b** with quaternary triphenylphosphonium bromide groups, and Mg^{II} porphyrin **1d** was more active than Zn^{II} porphyrin **1c**. With **2a** as a substrate, **1d** showed the highest catalytic activity, with a turnover number (TON) of 103,000 and a turnover frequency (TOF) of 12,000 h^{-1} under

Received: July 28, 2014
Published: September 30, 2014

   dx.doi.org/10.1021/ja507665a | J. Am. Chem. Soc. 2014, 136, 15270−15279

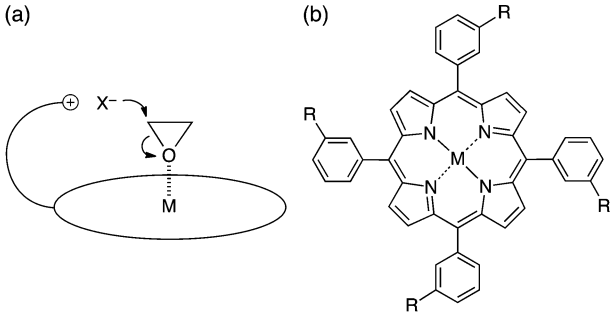

1a: M = Zn, R = $O(CH_2)_6P^+Ph_3Br^-$
1b: M = Mg, R = $O(CH_2)_6P^+Ph_3Br^-$
1c: M = Zn, R = $O(CH_2)_6N^+Bu_3Br^-$
1d: M = Mg, R = $O(CH_2)_6N^+Bu_3Br^-$
1e: M = Mg, R = $O(CH_2)_8N^+Bu_3Br^-$
1f: M = Mg, R = $O(CH_2)_4N^+Bu_3Br^-$
1g: M = Mg, R = $O(CH_2)_6$-N⁺ Br^-
1h: M = Mg, R = $O(CH_2)_6N^+Bu_3Cl^-$
1i: M = Mg, R = $O(CH_2)_6N^+Bu_3I^-$
1j: M = Mg, R = $O(CH_2)_6N^+Et_3Br^-$
1k: M = Mg, R = $O(CH_2)_6N^+Pr_3Br^-$
1l: M = Mg, R = $O(CH_2)_6N^+Hex_3Br^-$
1m: M = Mg, R = $O(CH_2)_6N^+Oct_3Br^-$
1n: M = Mg, R = $O(CH_2)_6NEt_2$

Figure 1. (a) Cooperative activation of epoxide with a bifunctional catalyst. (b) Bifunctional catalysts **1**.

solvent-free conditions (Scheme 1). In contrast, a binary catalytic system composed of (5,10,15,20-tetraphenylporphyrinato)magnesium(II) (Mg(TPP)) and tetrabutylammonium bromide (TBAB) showed much lower catalytic activity (TON = 5,000) under otherwise identical reaction conditions. These results clearly indicate the importance of cooperation between the two functional groups in the same molecule. Comparison of catalysts **1d–f**, which have different alkyl chain (linker) lengths, revealed that the catalytic activities decreased slightly in the order **1d** > **1e** ≈ **1f** (C6 > C8 ≈ C4). Catalyst **1g**, which has the alkylpyridinium bromide groups, showed much lower activity because of the poor nucleophilicity of the Br^- ion of the tight ion pair and the low solubility of **1g** in epoxide **2a**.[7]

Scheme 1. Synthesis of Cyclic Carbonate 3 from Epoxide 2 and CO_2

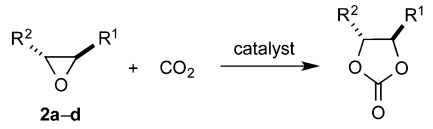

2a–d **3a–d**

a: R^1 = Bu, R^2 = H (**1d**: TON = 103,000, TOF = 12,000 h^{-1})
b: R^1 = Ph, R^2 = H
c: R^1 = Bu, R^2 = D
d: R^1 = Me, R^2 = H

Here, we studied bifunctional catalysts **1** in more detail. We conducted further structural optimization by synthesizing **1h–m**, which have different ion pairs, and **1n**, which has the diethylamino groups. We investigated the reaction mechanism by changing the CO_2 pressure (concentration) and by carrying out the reaction with ^{18}O-labeled CO_2 and D-labeled epoxide. Density functional theory (DFT) calculations were conducted to gain additional insight into the catalytic mechanism. These mechanistic studies have revealed the molecular behavior of highly active bifunctional catalysts **1** cooperatively using the flexible organocatalytic group and the Lewis acidic metal center under solvent-free conditions. The present study is also useful for the design of new catalysts as well as the understanding of congener catalysts.[10]

RESULTS AND DISCUSSION

Structural Optimization by Tuning the Pendent Nucleophilic Group. We optimized the structure of catalysts **1** by synthesizing a series of new derivatives (**1h–m**, Figure 1) and evaluating their catalytic activity for **2a** (Scheme 1). First, the effect of the X^- anion on the catalytic activity was examined (Table 1). The catalytic activities of **1d**, **1h**, and **1i**, which bear

Table 1. Effect of Counter Anion on Catalytic Activity[a]

entry	catalyst	yield (%)[b]	TON
1[c]	**1d**	99	19,800
2[c]	**1h**	48	9,600
3[c]	**1i**	7	1,400
4[d]	Mg(TPP) + TBAB	78	3,900
5[d]	Mg(TPP) + TBAC	75	3,800
6[d]	Mg(TPP) + TBAI	20	1,000
7[e]	TBAB	71	14
8[e]	TBAC	99	20
9[e]	TBAI	55	11

[a]Conditions: **2a** (1.00 g, 10.0 mmol), catalyst (indicated below), CO_2 (1.7 MPa), 120 °C, 3 h, in a 30 mL autoclave. [b]Determined by ^1H NMR using 2-methoxynaphthalene as an internal standard. [c]Catalyst **1** (0.005 mol %). [d]Mg(TPP) (0.02 mol %), quaternary ammonium salts (0.08 mol %). [e]Quaternary ammonium salts (5 mol %).

Br^-, Cl^-, and I^- ions, respectively, increased in the order **1i** < **1h** < **1d** (I^- < Cl^- < Br^-; entries 1–3). In general, Cl^- has the highest nucleophilicity in aprotic solvents, whereas I^- has the highest leaving ability.[11] Our results indicate that both the nucleophilicity and the leaving ability of the X^- anion are important for the catalytic activity of **1**, although the former seems to be more important because **1h** is more active than **1i**. For comparison, we also evaluated the catalytic activities of TBAB, tetrabutylammonium chloride (TBAC), and tetrabutylammonium iodide (TBAI) both in the presence and in the absence of Mg(TPP) (entries 4–9). In the binary catalytic systems, there was little or no difference in catalytic activity between TBAB and TBAC (entries 4 and 5). However, when the quaternary ammonium salts were used alone, TBAC showed the highest catalytic activity (compare entries 7–9). These results can be explained as follows: in the absence of the Lewis acid, nucleophilic attack of Br^- on the epoxide was slower than that of Cl^- because Br^- is intrinsically less nucleophilic than Cl^-; but in the presence of Mg(TPP), the ring-opening of the epoxide by Br^- was more effectively accelerated by the metal coordination. The ring-opening activity of **1d** was further enhanced by structure-specific synergy between the Lewis acid (Mg^{II}) and base (Br^-), which was revealed by DFT calculations as described later.

Next we tuned the tetraalkylammonium cation moiety, which can be expected to affect the nucleophilicity of the X^- anion (Table 2). Although bifunctional catalysts **1k–m** were only slightly less active than **1d**, **1j** showed somewhat lower activity. The less bulky triethylammonium cation in this catalyst may have formed a tighter ion pair with Br^-, thus decreasing its nucleophilicity. This result is similar to the previously reported results indicating that catalyst **1g**, bearing the alkylpyridinium bromide groups, showed low activity because the alkylpyridinium cation is less bulky than tetraalkylammonium cations.[7]

To evaluate the advantage conferred by the Br^- anion of **1d**, we examined **1n**, which has the diethylamino groups instead of quaternary ammonium salts. We anticipated that **1n** would

dx.doi.org/10.1021/ja507665a | J. Am. Chem. Soc. 2014, 136, 15270–15279

Table 2. Effect of Counter Cation on Catalytic Activity[a]

entry	catalyst	yield (%)[b]	TON
1	**1d**	68	34,000
2	**1j**	56	28,000
3	**1k**	67	33,500
4	**1l**	66	33,000
5	**1m**	65	32,500

[a]Conditions: **2a** (1.00 g, 10.0 mmol), catalyst **1** (0.002 mol %), CO_2 (1.7 MPa), 120 °C, 3 h, in a 30 mL autoclave. [b]Determined by ^{1}H NMR using 2-methoxynaphthalene as an internal standard.

show lower activity than **1d** or **1j** because the nucleophile (the amino group) of **1n** must be connected to the substrate via a covalent bond with some strain during catalysis. Indeed, the **1n**-catalyzed reaction of **2a** (0.005 mol %, 1.7 MPa CO_2, 120 °C, 3 h) gave **3a** in only 15% yield (compared to 99% for **1d** and 79% for **1j** under otherwise identical conditions). This result clearly demonstrates the superiority of the tetraalkylammonium bromide (ion pair) over the amino group as an organocatalytic site.

Based on all the results shown above, we designed and synthesized Mg^{II} porphyrin **1o** with eight tetraalkylammonium bromide groups (Figure 2). Although we were concerned about

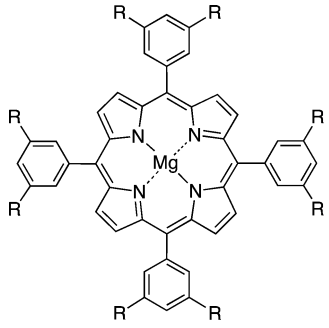

Figure 2. Bifunctional catalyst **1o**.

the poor solubility of **1o** in epoxide **2a** because of the eight ion pairs and higher molecular symmetry, fortunately, **1o** was soluble in **2a** and exhibited even higher catalytic activity than **1d** (Table 3, entries 1–4). The maximum TOF and TON for

Table 3. Comparison of Catalytic Activities of 1d and 1o[a]

entry	catalyst	loading (mol %)	time (h)	yield (%)[b]	TON
1	**1d**	0.003	1	36	12,000
2	**1o**	0.003	1	57	19,000
3	**1d**	0.0008	24	82	103,000
4	**1o**	0.0008	24	95	119,000
5	**1o**	0.0005	24	69	138,000

[a]Conditions: **2a** (1.00 g, 10.0 mmol), catalyst **1** (indicated above), CO_2 (1.7 MPa), 120 °C, in a 30 mL autoclave. [b]Determined by ^{1}H NMR using 2-methoxynaphthalene as an internal standard.

1o reached 19,000 h^{-1} and 138,000, respectively (entries 2 and 5), which are the highest values for the reaction of epoxides with CO_2 into cyclic carbonates to the best of our knowledge.

Effect of CO_2 Pressure. We investigated the effect of CO_2 pressure on the **1d**-catalyzed reaction in a stainless steel autoclave with a sapphire window so that we could observe how the reaction proceeded under solvent-free conditions. The autoclave was charged with **2a**, **1d** (0.005 or 0.002 mol %), and CO_2, and then the mixture was heated with stirring at 100 °C for 3 h (Figure 3). The yields remained nearly constant at initial

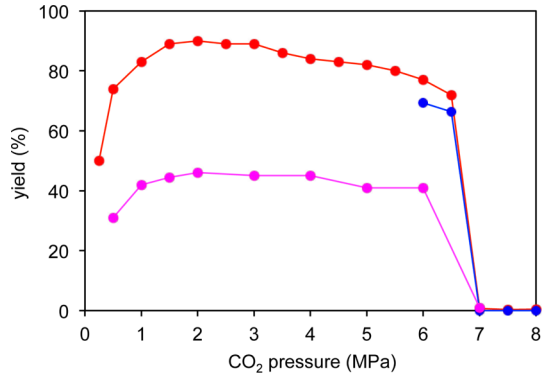

Figure 3. Effect of CO_2 pressure. Conditions: **2a** (1.00 g, 10.0 mmol), catalyst **1d** (red and blue: 0.005 mol %, magenta: 0.002 mol %), additive **3a** (red and magenta: 0 mol %, blue: 20 mol %), CO_2 (initial pressure indicated above), 100 °C, 3 h, in a 35 mL stainless steel autoclave with a sapphire window. The yield was determined by ^{1}H NMR using 2-methoxynaphthalene as an internal standard.

CO_2 pressures in the range of 1–6 MPa, suggesting that CO_2 was not involved in the rate-determining step in this pressure range. Interestingly, almost no reaction proceeded in supercritical CO_2 ($scCO_2$) at above 7 MPa of initial CO_2 pressure. Epoxide **2a** dissolved in $scCO_2$, whereas catalyst **1d** did not.[12] When the initial CO_2 pressure was 6–6.5 MPa, CO_2 was partially liquid at room temperature but changed to $scCO_2$ upon heating to 100 °C; during the heating period, **3a** accumulated at the bottom of the autoclave, and **1d** dissolved in the **3a**, which appeared to promote the reaction. In contrast, when 0.25–5.5 MPa CO_2 was heated to 100 °C, CO_2 remained as a gas, substrate **2a** remained as a liquid, and **1d** dissolved in it. These results suggest that dissolution of **1d** in the epoxide or the cyclic carbonate was the key to the reaction. In view of these results, we decided to use **3a** (20 mol %) as an additive for the solubilization of **1d**, and we carried out the reaction in $scCO_2$ (Figure 3). At a CO_2 pressure of >7 MPa CO_2, **1d** and **3a** dissolved completely in the $scCO_2$,[12] but no reaction proceeded. Dilution of the epoxide and **1d** in $scCO_2$ likely contributed to the drop in reaction rate.[13]

Catalytic Cycle. To determine the order of reaction with respect to catalyst **1d**, we examined the dependence of the conversion on catalyst loading. The reactions of **2a** with CO_2 (1.7 MPa) were conducted with varying amounts of **1d** at 120 °C for 1 h. The results are shown in Figure 4. Clearly, the conversion of **2a** at 1 h, which is proportional to the reaction rate, is proportional to the amount (concentration) of **1d**. Therefore, the kinetic order with respect to **1d** is 1, and one catalyst molecule is involved in the rate-determining step.

To investigate the reaction mechanism in detail, we used ^{18}O-labeled CO_2 in the **1d**-catalyzed reaction of styrene oxide (**2b**) (Scheme 2). The Br^- ion can attack either on the less hindered side of **2b** (path B, β attack) or on the more hindered side of **2b** (path A, α attack), giving two regioisomeric cyclic carbonates **3b**, which can be converted to benzaldehyde. Mass spectrometric analysis of the benzaldehyde indicated that the signal ratio of the products of path B and path A was 99:1 (see the Supporting Information). This high β selectivity for **2b** is

dx.doi.org/10.1021/ja507665a | J. Am. Chem. Soc. 2014, 136, 15270–15279

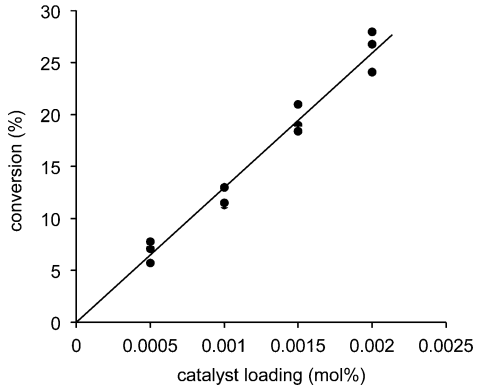

Figure 4. Determination of the reaction order with respect to catalyst **1d**. The experiments were done in triplicate.

Scheme 2. Investigation of the Reaction Mechanism by Using ^{18}O-Labeled CO_2[a]

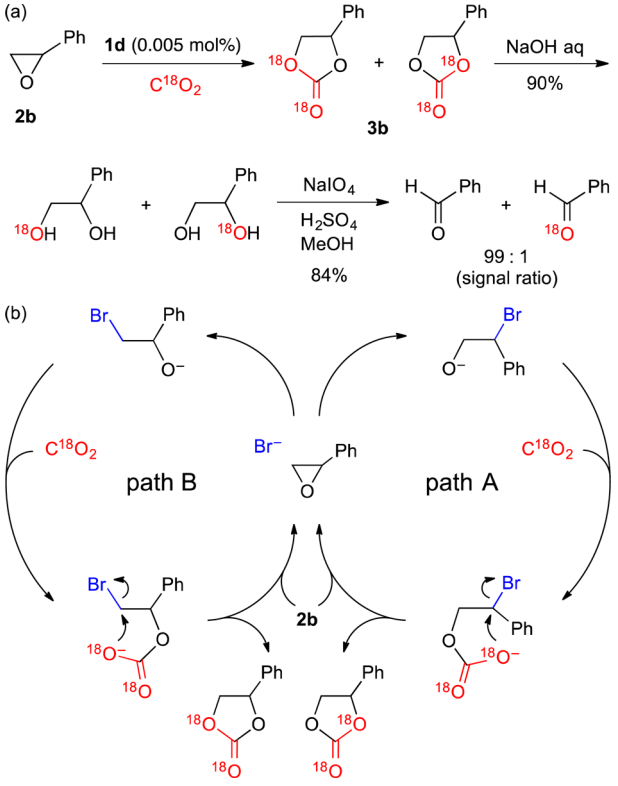

[a](a) Synthesis and analysis of ^{18}O-labeled cyclic carbonate **3b**. (b) Two possible catalytic cycles: nucleophilic attack by the Br^- ion on the less hindered side of **2b** (path B, β attack) and more hindered side of **2b** (path A, α attack).

surprising because Darensbourg, Lu, and co-workers have reported that the control of regioselectivity is difficult in the copolymerization of **2b** with CO_2.[3c,d] In addition, Kleij, Bo, and co-workers have reported that the α pathway is predominant in the conversion of **2b** into **3b** with a Zn(salphen)/TBAI catalytic system.[4l] It is believed that in most catalytic systems, terminal epoxides with electron-donating substituents favor β attack, while those with electron-withdrawing substituents, such as **2b**, undergo α attack but with low selectivity. Therefore, the high β selectivity of **1d** toward **2b**, which has been revealed by the isotope experiment with ^{18}O-labeled CO_2 (Scheme 2), is unusual and significant.[14]

Next, we determined whether the epoxide or CO_2 was initially attacked by the Br^- ion, by investigating the reaction of *trans*-deuterated epoxide **2c** (Scheme 3).[15] Attack of the Br^- ion on the epoxide (path B) would afford *trans*-**3c** (retention of configuration) via two inversions, whereas attack of the Br^- ion on CO_2 (path C) would afford *cis*-**3c** (inversion of configuration). Analysis of the product mixture by ^{1}H NMR indicated that *trans*-**3c** and *cis*-**3c** were produced in a ratio of 99:1 (see the Supporting Information).

Scheme 3. (a) Investigation of the Reaction Mechanism by Using Deuterated Epoxide *trans*-2c and (b) Two Possible Catalytic Cycles via the Nucleophilic Attack of Epoxide (path B) or CO_2 (path C) by the Br^- Ion

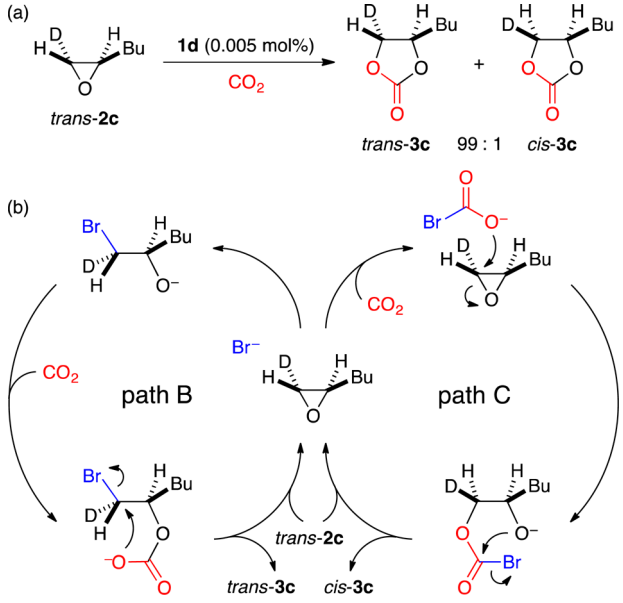

On the basis of the results of these mechanistic studies, we propose the catalytic cycle shown in Scheme 4. After coordination of the epoxide with the metal atom, nucleophilic attack by the Br^- ion on the less hindered side of the epoxide

Scheme 4. A Proposed Catalytic Cycle

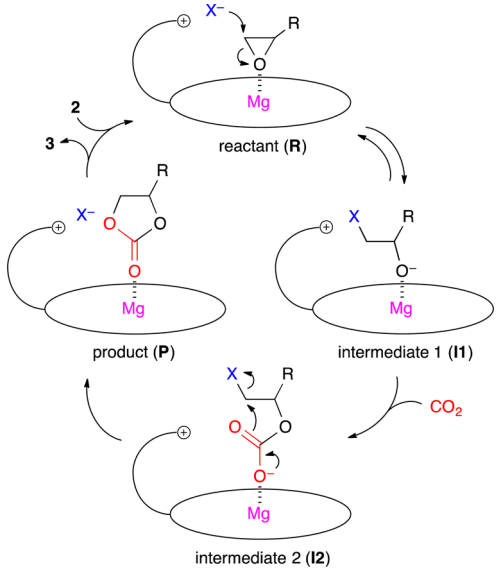

dx.doi.org/10.1021/ja507665a | J. Am. Chem. Soc. 2014, 136, 15270−15279

affords an alkoxide anion via a ring-opening reaction,[16] which is followed by CO_2 insertion and ring closure to form the cyclic carbonate and regenerate **1d**.

DFT Calculations. To gain deeper insight into the reaction mechanism, we performed DFT calculations along the proposed reaction pathway (Scheme 4). To investigate the effect of the X^- anion on catalytic activity, we used monosubstituted porphyrins **1d′**, **1h′**, and **1i′** (Figure 5) as

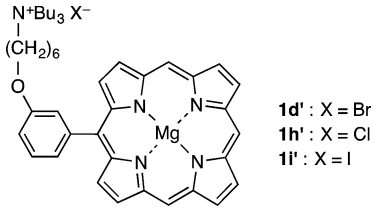

Figure 5. Model catalysts for DFT calculations.

models for catalyst **1d**, **1h**, and **1i**, respectively, and we used epoxide **2d** as a substrate (Scheme 1). The potential energy profiles calculated for the reactions catalyzed by **1d′**, **1h′**, and **1i′** are shown in Figure 6. The intermediate and transition-state structures in the **1d′**-catalyzed reaction are shown in Figure 7, and those for **1h′** and **1i′** are given in the Supporting Information.

Interestingly, the quaternary ammonium (QA) cation carries the positive charges on the H atoms, but not on the central N atom (Figure 7), and the positively charged H atoms form an anion-binding site. As represented by Figure 7a, the X^- anion in reactant complex **R** is stabilized by the positive charges distributed over the QA cation and is poised to attack epoxide **2d**. Nucleophilic attack by the X^- anion gives intermediate **I1** via transition state **I1_TS** (Figure 7b,c). The activation energies (E_a) are 13.5, 16.1, and 20.2 kcal/mol for the reactions with **1d′**, **1h′**, and **1i′**, respectively, which suggests that the nucleophilicity of the X^- anion in **1** increases in the order I^- < Cl^- < Br^- (Figure 6). Note that the usual order of the nucleophilicities of Br^- and Cl^- is reversed in this case; the nucleophilicity of "naked" X^- anions in polar aprotic solvents generally increases with basicity: I^- < Br^- < Cl^-.[11,17]

The X^- anion in **1** is not "naked" but "solvated by the tethered QA cation" so that the nucleophilicity of the X^- anion can be affected by the tethered QA cation. Therefore, the reversal in nucleophilicity occurred probably because the QA cation in **1d′** stabilizes Br^- with the best complementarity throughout the nucleophilic attack, especially in the transition state; see the concave anion-binding site that is complementary to the Br^- ion (Figure 7b). This stabilization can be deduced by comparing the shortest distances between the QA cation and the X^- anions in transition state **I1_TS**. The shortest distance between Br^- and H(QA) in **1d′** is 2.67 Å (Figure 7b), whereas that between Cl^- and H(QA) in **1h′** is 2.69 Å and that between I^- and H(QA) in **1i′** is 3.48 Å (Supporting Information). Because the ionic radii of the X^- anions increase in the order Cl^- < Br^- < I^-, the shortest distance between Br^- and H(QA) (2.67 Å) strongly suggests that tight and attractive interactions between Br^- and the QA cation stabilize the transition state.

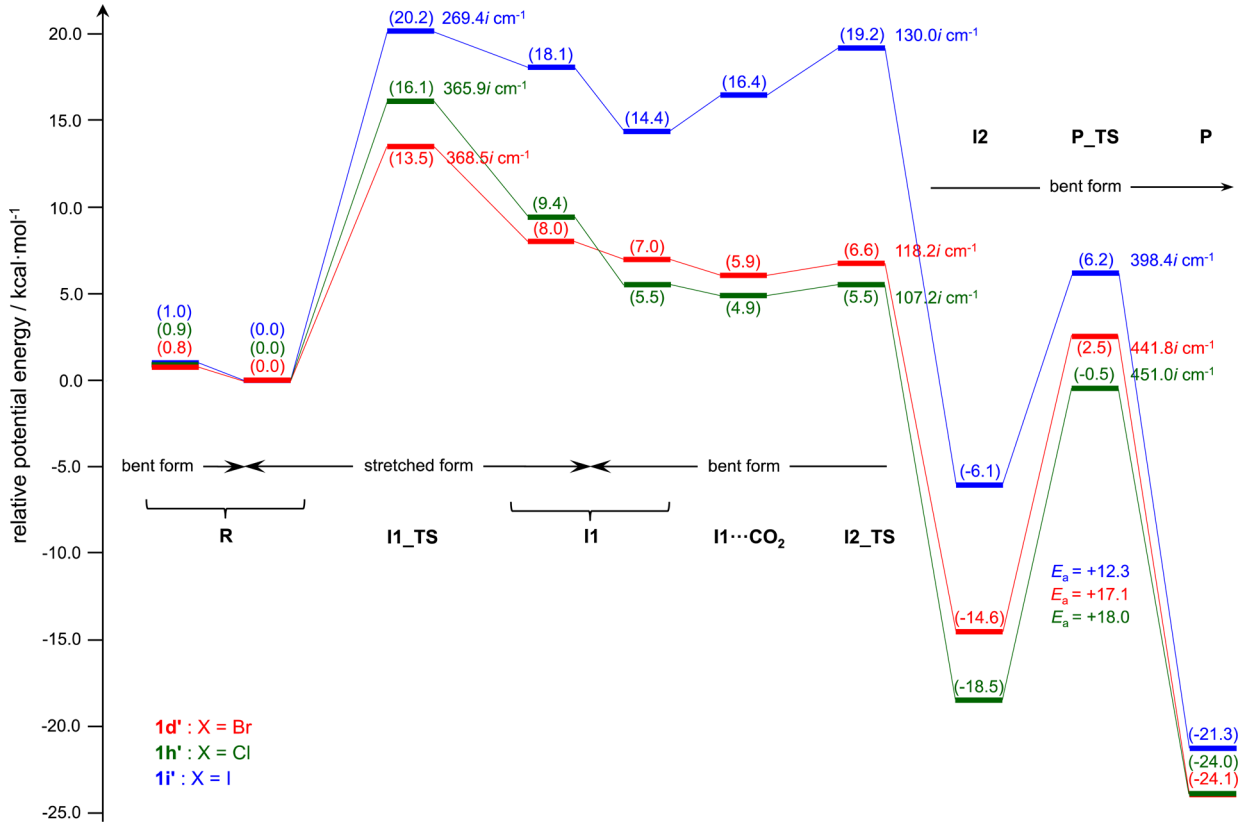

Figure 6. Potential energy profiles for the **1d′**, **1h′**, and **1i′**-catalyzed reactions of **2d** with CO_2. Computations were performed at the B3LYP/6-31G* level with the self-consistent reaction field (SCRF) method (Et_2O). The relative energies based on reactant **R** (stretched form) are given in kcal/mol. The energy of CO_2 is included in the former steps where CO_2 does not appear explicitly. The stretched and bent forms designated here can be seen in Figure 7.

dx.doi.org/10.1021/ja507665a | J. Am. Chem. Soc. 2014, 136, 15270−15279

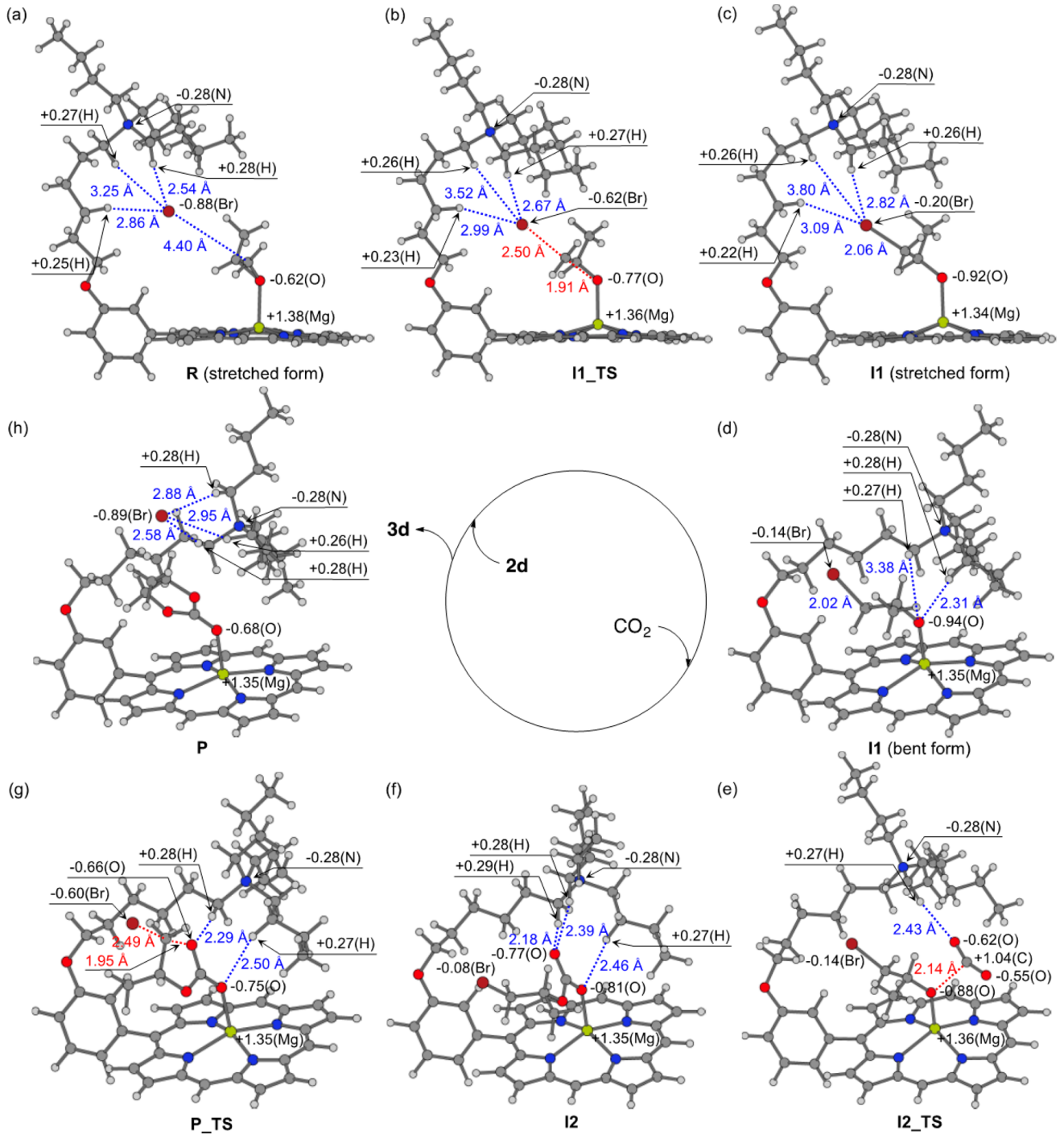

Figure 7. Optimized structures of (a) reactant **R** (stretched form), (b) transition state **I1_TS**, (c) **I1** (stretched form), (d) **I1** (bent form), (e) transition state **I2_TS**, (f) **I2**, (g) transition state **P_TS**, and (h) product **P** in the **1d′**-catalyzed reaction of **2d** with CO_2.

The same tendency can be seen for the distances between X^- and H(QA) of the linker moiety, which is a part of the concave anion-binding site: 2.99 Å (Figure 7b), 3.11 Å, and 3.84 Å (Supporting Information) for **1d′**, **1h′**, and **1i′**, respectively. These observations strongly suggest that the linker length is important for the transition-state stabilization, which was observed experimentally, **1d** (C6) > **1e** (C8) ≈ **1f** (C4), although the difference was not so critical probably because of the flexible alkyl chains.[7] Furthermore, these attractive interactions between the QA cation and the Br atom appear to be more or less retained in intermediate **I1** (stretched form) (Figure 7c, 2.82 and 3.09 Å).

It is also interesting to compare the conformational changes of the QA cations in **1d′**, **1h′**, and **1i′** in going from **R** to **I1** (stretched form). We used the N(QA)−O(**2d**) distance to estimate the conformational change of the QA cation. In the case of **1d′**, the N(QA)−O(**2d**) distance changes from 9.30 Å in **R** to 8.54 Å in the stretched form of **I1**; that is, the N(QA) atom in **1d′** gets closer to **2d** by 0.76 Å. The corresponding values in **1h′** and **1i′** are 1.40 and 1.11 Å, respectively. Clearly, **1d′** experiences the smallest conformational change. The

dx.doi.org/10.1021/ja507665a | J. Am. Chem. Soc. 2014, 136, 15270−15279

smallest conformational change observed for **1d′** is a result of the best preorganization leading to the ring-opening reaction guided by the multipoint interactions described above. For more discussion of the origin of the reversed order of the nucleophilicities of Br^- and Cl^- in **1** see the Supporting Information.[17]

The charge on the Br atom changes from −0.88 in **R** to −0.20 in the stretched form of **I1**, whereas that on the O atom of **2d** changes from −0.62 in **R** to −0.92 in the stretched form of **I1**; this shift in negative charge from the Br atom to the O atom is facilitated by the partial emergence of the positively charged Mg atom from the porphyrin cavity (Figure 7a−c).[18] This shift in negative charge triggers the conversion of the stretched form of **I1** into a bent form in which the QA cation is closer to the negatively charged O atom of **2d** that has been ring-opened (2.31 Å; Figure 7d). To maximize these attractive interactions, the methyl group of **2d**, which is directed upward in the stretched form of **I1** (Figure 7c), points away from the QA cation in the bent form of **I1** (Figure 7d).

After CO_2 has been weakly bound to give complex **I1**···$\mathbf{CO_2}$ (not shown in Figure 7), the C−O bond forms via transition state **I2_TS**, in which a negatively charged O atom of CO_2 is stabilized by the QA cation (Figure 7e). This reaction has a very small activation barrier (E_a = 0.6−0.7 kcal/mol for **1d′** and **1h′** and 2.8 kcal/mol for **1i′**; Figure 6). Formation of the C−O bond and coordination of the resulting carbonate anion to the Mg atom lead to intermediate **I2**, which is stabilized by multiple interactions between the carbonate anion and the QA cation in a bent conformation (Figure 7f). The QA cation interacts with the two negatively charged O atoms, with the shortest H(QA)−O(carbonate) distance being 2.18 Å. Electrostatic stabilization is clearly maximized by the conformational change of the QA cation. This CO_2 insertion reaction is very exothermic ($\Delta H^\circ \approx -20$ kcal/mol; Figure 6).[19]

The catalytic cycle is completed by an intramolecular S_N2 reaction that occurs via transition state **P_TS** and gives product **P** (Figure 7g,h). In transition state **P_TS**, the QA cation interacts tightly with the two negatively charged O atoms of the carbonate rather than with the leaving Br atom. The E_a values for the ring-closing reaction increase in the order **1i′** < **1d′** < **1h′**, and the ΔH° (absolute) values show the opposite trend (Figure 6). These trends are related to the strength of the C−X bonds. The average bond dissociation energies (D°) for the C−Cl, C−Br and C−I bonds are reported to be 95, 67, and 50 kcal/mol, respectively.[20] The E_a and ΔH° values for **1i′** are the smallest and the most negative, respectively, because the C−I bond is the weakest of the C−X bonds. In contrast, **1h′** shows the largest E_a value and the least negative ΔH° value because the C−Cl bond is the strongest of the C−X bonds. The X^- anion regenerated in **P** interacts strongly with the QA cation. Replacement of cyclic carbonate **3d** with epoxide **2d** and a conformational change gives a stretched form of **R**.[21]

Because the highest energy transition state is generally the rate-determining step,[11] Figure 6 indicates that the rate-determining step involves transition state **I1_TS** in all cases. On the basis of the E_a values for **I1_TS**, we can predict that the catalytic activities of the three catalysts should increase in the order **1i′** (20.2 kcal/mol) < **1h′** (16.1 kcal/mol) < **1d′** (13.5 kcal/mol). This prediction agrees qualitatively with the yields shown in Table 1. Figure 6 also suggests that the CO_2 insertion reaction is not the rate-determining step because the E_a value for transition state **I2_TS** is very small in all cases, as described above, and because **I2_TS** is lower in energy than **I1_TS**. This prediction is supported by the fact that the yields were almost constant at 1−6 MPa CO_2 pressure (Figure 3). The final step is the ring closure of stable intermediate **I2**. Because the E_a values for transition state **P_TS** are relatively large (Figure 6), this step contributes to the whole reaction rate to some degree. To the best of our knowledge, the E_a value calculated for **1d′** (13.5 kcal/mol) is the smallest, which accords with the fact that **1d** and **1o** are the most active catalysts so far reported.

■ CONCLUSIONS

Chemical fixation of CO_2 is becoming increasingly important. Here, we describe the structural optimization and detailed mechanistic analysis of highly active bifunctional catalysts **1**, which have a metal center and quaternary ammonium groups. Structural optimization of the organocatalytic moiety revealed that the combination of a tributylammonium cation and a Br^- ion was the best choice. A key to the solvent-free reactions was the solubility of the catalyst in the epoxide substrate or the cyclic carbonate product. The high catalytic activity of **1d** (TON = 103,000 and TOF = 12,000 h^{-1}) and **1o** (TON = 138,000 and TOF = 19,000 h^{-1}) is achieved by means of synergistic cooperation between a Lewis acid (Mg^{II}) and a base (Br^-) without self-quenching. On the basis of the results of experiments using ^{18}O-labeled CO_2 and D-labeled epoxide, we have proposed a mechanism for the reaction. The proposed reaction mechanism was supported by the results of DFT calculations. The activation energies (E_a) estimated for the rate-determining step were in good agreement with the experimentally observed trend for the catalytic activities of **1d**, **1h**, and **1i**. **1d** and **1o** are the most active catalysts so far reported, which has been supported by the E_a value calculated for **1d′** (13.5 kcal/mol), which is the smallest value. The cooperative effect of the two functional groups in **1** is the principal origin of the catalytic power. Although **1** was originally designed to activate the epoxide by orienting it in a near-attack conformation (Figure 1a), DFT calculations revealed that the flexible QA cation stabilized various anionic species generated during the catalytic cycle in an induced-fit manner, which is reminiscent of enzymatic catalysis. Synergistic multiple interactions accompanied by conformational changes play a pivotal role in bifunctional catalysts **1** orchestrating metal catalysis and organocatalysis.

■ EXPERIMENTAL SECTION

Synthesis of Catalysts. Bifunctional porphyrins **1h−o** were newly synthesized according to the previously reported methods.[7,22] The detailed procedures are given in the Supporting Information.

Effect of CO_2 Pressure. A 35 mL stainless steel autoclave with a sapphire window was charged with epoxide **2a** (1.00 g, 10.0 mmol), **3a** (0 or 20 mol %), **1d** (1.05 mg, 0.501 μmol, 0.005 mol % or 0.420 mg, 0.201 μmol, 0.002 mol %), and then CO_2. The mixture was heated with stirring at 100 °C for 3 h. The reactor was cooled in an ice bath for 30 min, and excess CO_2 was released carefully. The crude product was dissolved in Et_2O, and the solution was concentrated. The NMR yield was determined by using 2-methoxynaphthalene as an internal standard.

Synthesis of ^{18}O-Labeled Cyclic Carbonate 3b. A 30 mL stainless steel autoclave was charged with styrene oxide (**2b**) (2.40 g, 20.0 mmol), **1d** (2.10 mg, 1.00 μmol, 0.005 mol %), and then ^{18}O-labeled CO_2 (0.75 MPa). The mixture was stirred at 120 °C for 24 h. The reactor was cooled in an ice bath for 30 min, and excess CO_2 was released carefully. Purification by silica gel column chromatography (hexane/EtOAc (3:1)) gave ^{18}O-labeled **3b** as a colorless oil (1.87 g, 55%). ^1H NMR ($CDCl_3$, 600 MHz) δ 4.35 (t, J = 8.2 Hz, 1H), 4.80 (t, J = 8.2 Hz, 1H), 5.68 (t, J = 8.2 Hz, 1H), 7.36−7.38 (m, 2H), 7.42−

dx.doi.org/10.1021/ja507665a | J. Am. Chem. Soc. 2014, 136, 15270−15279

7.47 (m, 3H); ^{13}C NMR ($CDCl_3$, 150 MHz) δ 71.1, 78.0, 125.8, 129.2, 129.7, 135.8, 154.8; MS (EI) calcd for $C_9H_8O^{18}O_2$: 168.1; found: 168.1 (M^+).

Conversion of ^{18}O-Labeled 3b into Benzaldehyde. A mixture of ^{18}O-labeled **3b** (934 mg, 5.56 mmol) and 2 M NaOH (11 mL) was stirred at room temperature for 2 h. After neutralization, the product was extracted with EtOAc and washed with brine. The mixture was dried over Na_2SO_4 and concentrated. Purification by silica gel column chromatography (hexane/EtOAc (1:2)) gave the product as a white solid (699 mg, 90%). MS (EI) calcd for $C_8H_{10}O^{18}O$: 140.1; found: 140.1 (M^+). A solution of ^{18}O-labeled 1-phenyl-1,2-ethanediol (210 mg, 1.50 mmol) in MeOH (5 mL) was stirred at 40 °C for 10 min under Ar. $NaIO_4$ (353 mg, 1.65 mmol) and 0.5 M H_2SO_4 (18 mL) were added, and the mixture was stirred at 40 °C for 20 min. The product was extracted with Et_2O. The mixture was dried over Na_2SO_4 and concentrated. Purification by distillation (5 mmHg, 60 °C) gave benzaldehyde (134 mg, 84%), which was subjected to mass spectrometry. MS (EI) calcd for C_7H_6O: 106.0; found: 106.0 (M^+); MS (EI) calcd for $C_7H_6{}^{18}O$: 108.0; found: 108.0 (M^+).

Synthesis of *trans*-Deuterated Cyclic Carbonate 3c. A 30 mL stainless steel autoclave was charged with *trans*-deuterated epoxide **2c** (984 mg, 9.73 mmol),[15] **1d** (1.05 mg, 0.501 μmol, 0.005 mol %), and then CO_2 (1.5 MPa). The mixture was heated with stirring at 120 °C for 6 h. The reactor was cooled in an ice bath for 30 min, and excess CO_2 was released carefully. Purification by silica gel column chromatography (hexane/EtOAc (3:1)) gave *trans*-**3c** as a colorless oil (1.02 g, 72%). ^{1}H NMR ($CDCl_3$, 600 MHz) δ 0.93 (t, J = 7.2 Hz, 3H), 1.32−1.49 (m, 4H), 1.66−1.72 (m, 1H), 1.79−1.85 (m, 1H), 4.06 (d, J = 7.0 Hz, 1H), 4.70 (q, J = 7.0 Hz, 1H); ^{13}C NMR ($CDCl_3$, 150 MHz) δ 13.5, 22.0, 26.2, 33.2, 68.9 (t, J_{CD} = 23.7 Hz), 76.9, 155.0; IR (neat) 2962, 2936, 2870, 1794, 1543, 1466, 1366, 1304, 1177, 1061, 775, 714 cm^{-1}.

Computational Details. DFT calculations were performed along the proposed reaction pathway (Scheme 4). Monosubstituted porphyrins **1d**′, **1h**′, and **1i**′ (Figure 5) were employed as model catalysts for **1d**, **1h**, and **1i**, respectively, while epoxide **2d** was employed as a substrate (Scheme 1). Computations were performed at the B3LYP[23]/6-31G*[24] level. The self-consistent reaction field (SCRF) method with the polarizable continuum model (PCM)[25] was adopted to take into account of the solvation effect. The PCM parameters for Et_2O, which is expected to have a dielectric constant similar to that of epoxide, was used.[26] The harmonic frequency and normal mode were calculated to verify the transition-state structures. Natural population analysis (NPA)[27] was done to calculate the natural atomic charges. Computations were performed with Gaussian 09 program.[28]

■ ASSOCIATED CONTENT

Supporting Information

Synthesis of **1h−o**, ^{1}H and ^{13}C NMR spectra, isotope experiments, determination of binding constants, computational details, and complete ref 28. This material is available free of charge via the Internet at http://pubs.acs.org.

■ AUTHOR INFORMATION

Corresponding Authors

ema@cc.okayama-u.ac.jp

hasegawa@cat.hokudai.ac.jp

Notes

The authors declare no competing financial interest.

■ ACKNOWLEDGMENTS

This work was supported by ENEOS Hydrogen Trust Fund, Adaptable and Seamless Technology Transfer Program through Target-Driven R&D (A-STEP, Exploratory Research) from Japan Science and Technology Agency (JST), and Okayama Foundation for Science and Technology. NMR spectra were measured at the SC-NMR Laboratory of Okayama University. Computations were partly carried out at RCCS (Okazaki, Japan) and ACCMS (Kyoto University). We thank Prof. A. Osuka (Kyoto University) for ESI-MS measurements.

■ REFERENCES

(1) Reviews: (a) Sakakura, T.; Choi, J.-C.; Yasuda, H. *Chem. Rev.* **2007**, *107*, 2365−2387. (b) Darensbourg, D. J. *Chem. Rev.* **2007**, *107*, 2388−2410. (c) Sakakura, T.; Kohno, K. *Chem. Commun.* **2009**, 1312−1330. (d) North, M.; Pasquale, R.; Young, C. *Green Chem.* **2010**, *12*, 1514−1539. (e) Riduan, S. N.; Zhang, Y. *Dalton Trans.* **2010**, *39*, 3347−3357. (f) Klaus, S.; Lehenmeier, M. W.; Anderson, C. E.; Rieger, B. *Coord. Chem. Rev.* **2011**, *255*, 1460−1479. (g) Cokoja, M.; Bruckmeier, C.; Rieger, B.; Herrmann, W. A.; Kühn, F. E. *Angew. Chem., Int. Ed.* **2011**, *50*, 8510−8537. (h) Tsuji, Y.; Fujihara, T. *Chem. Commun.* **2012**, *48*, 9956−9964. (i) Darensbourg, D. J.; Wilson, S. J. *Green Chem.* **2012**, *14*, 2665−2671. (j) Omae, I. *Coord. Chem. Rev.* **2012**, *256*, 1384−1405. (k) Kielland, N.; Whiteoak, C. J.; Kleij, A. W. *Adv. Synth. Catal.* **2013**, *355*, 2115−2138. (l) Maeda, C.; Miyazaki, Y.; Ema, T. *Catal. Sci. Technol.* **2014**, *4*, 1482−1497.

(2) Various transformations of CO_2: (a) Kayaki, Y.; Yamamoto, M.; Ikariya, T. *Angew. Chem., Int. Ed.* **2009**, *48*, 4194−4197. (b) Riduan, S. N.; Zhang, Y.; Ying, J. Y. *Angew. Chem., Int. Ed.* **2009**, *48*, 3322−3325. (c) Zhang, W.-Z.; Li, W.-J.; Zhang, X.; Zhou, H.; Lu, X.-B. *Org. Lett.* **2010**, *12*, 4748−4751. (d) Gu, L.; Zhang, Y. *J. Am. Chem. Soc.* **2010**, *132*, 914−915. (e) Berkefeld, A.; Piers, W. E.; Parvez, M. *J. Am. Chem. Soc.* **2010**, *132*, 10660−10661. (f) Mizuno, H.; Takaya, J.; Iwasawa, N. *J. Am. Chem. Soc.* **2011**, *133*, 1251−1253. (g) Ohmiya, H.; Tanabe, M.; Sawamura, M. *Org. Lett.* **2011**, *13*, 1086−1088. (h) Inamoto, K.; Asano, N.; Nakamura, Y.; Yonemoto, M.; Kondo, Y. *Org. Lett.* **2012**, *14*, 2622−2625. (i) Fujihara, T.; Nogi, K.; Xu, T.; Terao, J.; Tsuji, Y. *J. Am. Chem. Soc.* **2012**, *134*, 9106−9109. (j) Dai, Y.; Feng, X.; Wang, B.; He, R.; Bao, M. *J. Organomet. Chem.* **2012**, *696*, 4309−4314. (k) Mita, T.; Michigami, K.; Sato, Y. *Org. Lett.* **2012**, *14*, 3462−3465. (l) Mita, T.; Sugawara, M.; Hasegawa, H.; Sato, Y. *J. Org. Chem.* **2012**, *77*, 2159−2168. (m) Ishida, N.; Shimamoto, Y.; Murakami, M. *Angew. Chem., Int. Ed.* **2012**, *51*, 11750−11752. (n) León, T.; Correa, A.; Martin, R. *J. Am. Chem. Soc.* **2013**, *135*, 1221−1224. (o) Ishida, T.; Kikuchi, S.; Tsubo, T.; Yamada, T. *Org. Lett.* **2013**, *15*, 848−851. (p) Li, S.; Miao, B.; Yuan, W.; Ma, S. *Org. Lett.* **2013**, *15*, 977−979. (q) Yu, B.; Zhang, H.; Zhao, Y.; Chen, S.; Xu, J.; Huang, C.; Liu, Z. *Green Chem.* **2013**, *15*, 95−99. (r) Ueno, A.; Kayaki, Y.; Ikariya, T. *Green Chem.* **2013**, *15*, 425−430. (s) Correa, A.; León, T.; Martin, R. *J. Am. Chem. Soc.* **2014**, *136*, 1062−1069.

(3) Polycarbonate synthesis from epoxides and CO_2: (a) Nakano, K.; Hashimoto, S.; Nozaki, K. *Chem. Sci.* **2010**, *1*, 369−373. (b) Vagin, S. I.; Reichardt, R.; Klaus, S.; Rieger, B. *J. Am. Chem. Soc.* **2010**, *132*, 14367−14369. (c) Wu, G.-P.; Wei, S.-H.; Lu, X.-B.; Ren, W.-M.; Darensbourg, D. J. *Macromolecules* **2010**, *43*, 9202−9204. (d) Wu, G.-P.; Wei, S.-H.; Ren, W.-M.; Lu, X.-B.; Li, B.; Zu, Y.-P.; Darensbourg, D. J. *Energy Environ. Sci.* **2011**, *4*, 5084−5092. (e) Wu, G.-P.; Wei, S.-H.; Ren, W.-M.; Lu, X.-B.; Xu, T.-Q.; Darensbourg, D. J. *J. Am. Chem. Soc.* **2011**, *133*, 15191−15199. (f) Li, H.; Niu, Y. *Appl. Organometal. Chem.* **2011**, *25*, 424−428. (g) Nakano, K.; Kobayashi, K.; Nozaki, K. *J. Am. Chem. Soc.* **2011**, *133*, 10720−10723. (h) Kim, J. G.; Cowman, C. D.; LaPointe, A. M.; Wiesner, U.; Coates, G. W. *Macromolecules* **2011**, *44*, 1110−1113. (i) Widger, P. C. B.; Ahmed, S. M.; Coates, G. W. *Macromolecules* **2011**, *44*, 5666−5670. (j) Nakano, K.; Kobayashi, K.; Ohkawara, T.; Imoto, H.; Nozaki, K. *J. Am. Chem. Soc.* **2013**, *135*, 8456−8459. (k) Saini, P. K.; Romain, C.; Williams, C. K. *Chem. Commun.* **2014**, *50*, 4164−4167.

(4) Recent examples of metal complex catalysts: (a) Song, J.; Zhang, Z.; Hu, S.; Wu, T.; Jiang, T.; Han, B. *Green Chem.* **2009**, *11*, 1031−1036. (b) Qiao, K.; Ono, F.; Bao, Q.; Tomida, D.; Yokoyama, C. *J. Mol. Catal. A: Chem.* **2009**, *303*, 30−34. (c) Ulusoy, M.; Çetinkaya, E.; Çetinkaya, B. *Appl. Organometal. Chem.* **2009**, *23*, 68−74. (d) Meléndez, J.; North, M.; Villuendas, P. *Chem. Commun.* **2009**, 2577−2579. (e) Clegg, W.; Harrington, R. W.; North, M.; Pasquale, R.

Chem.—Eur. J. **2010**, *16*, 6828−6843. (f) Decortes, A.; Belmonte, M. M.; Benet-Buchholz, J.; Kleij, A. W. *Chem. Commun.* **2010**, *46*, 4580−4582. (g) Meléndez, J.; North, M.; Villuendas, P.; Young, C. *Dalton Trans.* **2011**, *40*, 3885−3902. (h) Ramidi, P.; Sullivan, S. Z.; Gartia, Y.; Munshi, P.; Griffin, W. O.; Darsey, J. A.; Biswas, A.; Shaikh, A. U.; Ghosh, A. *Ind. Eng. Chem. Res.* **2011**, *50*, 7800−7807. (i) Chen, F.; Li, X.; Wang, B.; Xu, T.; Chen, S.-L.; Liu, P.; Hu, C. *Chem.—Eur. J.* **2012**, *18*, 9870−9876. (j) Whiteoak, C. J.; Kielland, N.; Laserna, V.; Escudero-Adán, E. C.; Martin, E.; Kleij, A. W. *J. Am. Chem. Soc.* **2013**, *135*, 1228−1231. (k) Escárcega-Bobadilla, M. V.; Belmonte, M. M.; Martin, E.; Escudero-Adán, E. C.; Kleij, A. W. *Chem.—Eur. J.* **2013**, *19*, 2641−2648. (l) Castro-Gómez, F.; Salassa, G.; Kleij, A. W.; Bo, C. *Chem.—Eur. J.* **2013**, *19*, 6289−6298. (m) Babu, H. V.; Muralidharan, K. *Dalton Trans.* **2013**, *42*, 1238−1248. (n) Kim, J.; Kim, S.-N.; Jang, H.-G.; Seo, G.; Ahn, W.-S. *Appl. Catal. A: General* **2013**, *453*, 175−180. (o) Zalomaeva, O. V.; Chibiryaev, A. M.; Kovalenko, K. A.; Kholdeeva, O. A.; Balzhinimaev, B. S.; Fedin, V. P. *J. Catal.* **2013**, *298*, 179−185. (p) Kim, S. H.; Ahn, D.; Go, M. J.; Park, M. H.; Kim, M.; Lee, J.; Kim, Y. *Organometallics* **2014**, *33*, 2770−2775. (q) Castro-Osma, J. A.; Alonso-Moreno, C.; Lara-Sánchez, A.; Martinez, J.; North, M.; Otero, A. *Catal. Sci. Technol.* **2014**, *4*, 1674−1684.

(5) Recent examples of organocatalysts: (a) Sakai, T.; Tsutsumi, Y.; Ema, T. *Green Chem.* **2008**, *10*, 337−341. (b) Sun, J.; Zhang, S.; Cheng, W.; Ren, J. *Tetrahedron Lett.* **2008**, *49*, 3588−3591. (c) Motokura, K.; Itagaki, S.; Iwasawa, Y.; Miyaji, A.; Baba, T. *Green Chem.* **2009**, *11*, 1876−1880. (d) Tsutsumi, Y.; Yamakawa, K.; Yoshida, M.; Ema, T.; Sakai, T. *Org. Lett.* **2010**, *12*, 5728−5731. (e) Prasetyanto, E. A.; Ansari, M. B.; Min, B.-H.; Park, S.-E. *Catal. Today* **2010**, *158*, 252−257. (f) Zhou, H.; Wang, Y.-M.; Zhang, W.-Z.; Qu, J.-P.; Lu, X.-B. *Green Chem.* **2011**, *13*, 644−650. (g) Liang, S.; Liu, H.; Jiang, T.; Song, J.; Yang, G.; Han, B. *Chem. Commun.* **2011**, *47*, 2131−2133. (h) Han, L.; Choi, H.-J.; Choi, S.-J.; Liu, B.; Park, D.-W. *Green Chem.* **2011**, *13*, 1023−1028. (i) Aoyagi, N.; Furusho, Y.; Endo, T. *Chem. Lett.* **2012**, *41*, 240−241. (j) Yang, Z.-Z.; Zhao, Y.-N.; He, L.-N.; Gao, J.; Yin, Z.-S. *Green Chem.* **2012**, *14*, 519−527. (k) Song, Q.-W.; He, L.-N.; Wang, J.-Q.; Yasuda, H.; Sakakura, T. *Green Chem.* **2013**, *15*, 110−115. (l) Zhao, Y.; Yao, C.; Chen, G.; Yuan, Q. *Green Chem.* **2013**, *15*, 446−452. (m) Aoyagi, N.; Furusho, Y.; Endo, T. *J. Polym. Sci. A: Polym. Chem.* **2013**, *51*, 1230−1242. (n) Cheng, W.; Chen, X.; Sun, J.; Wang, J.; Zhang, S. *Catal. Today* **2013**, *200*, 117−124. (o) Chatelet, B.; Joucla, L.; Dutasta, J.-P.; Martinez, A.; Szeto, K. C.; Dufaud, V. *J. Am. Chem. Soc.* **2013**, *135*, 5348−5351. (p) Wang, Y.-B.; Sun, D.-S.; Zhou, H.; Zhang, W.-Z.; Lu, X.-B. *Green Chem.* **2014**, *16*, 2266−2272.

(6) (a) Aida, T.; Inoue, S. *J. Am. Chem. Soc.* **1983**, *105*, 1304−1309. (b) Kruper, W. J.; Dellar, D. V. *J. Org. Chem.* **1995**, *60*, 725−727. (c) Paddock, R. L.; Hiyama, Y.; McKay, J. M.; Nguyen, S. T. *Tetrahedron Lett.* **2004**, *45*, 2023−2026. (d) Srivastava, R.; Bennur, T. H.; Srinivas, D. *J. Mol. Catal. A: Chem.* **2005**, *226*, 199−205. (e) Jin, L.; Jing, H.; Chang, T.; Bu, X.; Wang, L.; Liu, Z. *J. Mol. Catal. A: Chem.* **2007**, *261*, 262−266. (f) Bai, D.; Wang, Q.; Song, Y.; Li, B.; Jing, H. *Catal. Commun.* **2011**, *12*, 684−688. (g) Ahmadi, F.; Tangestaninejad, S.; Moghadam, M.; Mirkhani, V.; Mohammadpoor-Baltork, I.; Khosropour, A. R. *Inorg. Chem. Commun.* **2011**, *14*, 1489−1493. (h) Wang, M.; She, Y.; Zhou, X.; Ji, H. *Chin. J. Chem. Eng.* **2011**, *19*, 446−451. (i) Anderson, C. E.; Vagin, S. I.; Xia, W.; Jin, H.; Rieger, B. *Macromolecules* **2012**, *45*, 6840−6849. (j) Wu, W.; Qin, Y.; Wang, X.; Wang, F. *J. Polym. Sci. A: Polym. Chem.* **2013**, *51*, 493−498.

(7) Ema, T.; Miyazaki, Y.; Koyama, S.; Yano, Y.; Sakai, T. *Chem. Commun.* **2012**, *48*, 4489−4491.

(8) Mizutani, T.; Ema, T.; Tomita, T.; Kuroda, Y.; Ogoshi, H. *J. Am. Chem. Soc.* **1994**, *116*, 4240−4250.

(9) (a) Konsler, R. G.; Karl, J.; Jacobsen, E. N. *J. Am. Chem. Soc.* **1998**, *120*, 10780−10781. (b) Breinbauer, R.; Jacobsen, E. N. *Angew. Chem., Int. Ed.* **2000**, *39*, 3604−3607. (c) Ema, T.; Tanida, D.; Matsukawa, T.; Sakai, T. *Chem. Commun.* **2008**, 957−959.

(10) Ema, T.; Miyazaki, Y.; Taniguchi, T.; Takada, J. *Green Chem.* **2013**, *15*, 2485−2492.

(11) For example, see: Smith, J. G. *Organic Chemistry*, 3rd ed.; McGraw-Hill: Singapore, 2011.

(12) (a) Chrastil, J. *J. Phys. Chem.* **1982**, *86*, 3016−3021. (b) Kawanami, H.; Sasaki, A.; Matsui, K.; Ikushima, Y. *Chem. Commun.* **2003**, 896−897.

(13) There is another possibility that **1d** was decomposed by $scCO_2$. To test this possibility, only **1d** was subjected to $scCO_2$ (8 MPa CO_2 initial pressure) at 100 °C for 1 h. After releasing the CO_2, **2a** and CO_2 (2 MPa) were added, and the mixture was heated with stirring at 100 °C for 3 h. As a result, **3a** was obtained in 66% yield. Therefore, this possibility was ruled out.

(14) Interestingly, DFT calculations strongly suggested that the regioselective ring-opening of **2d** is under kinetic control depending on the relative stability of the first transition state, whereas that of **2b** is under thermodynamic control depending on the relative stability of the first reaction intermediate, both of which favor the β pathway (path B). See the Supporting Information.

(15) Zhou, H.; Zhang, W.-Z.; Liu, C.-H.; Qu, J.-P.; Lu, X.-B. *J. Org. Chem.* **2008**, *73*, 8039−8044.

(16) When a mixture of epoxide **2a** and catalyst **1d** (0.005 mol%) was heated at 120 °C for 3 h under Ar (1.5 MPa), no reaction took place with **2a** recovered (90% yield), which suggests that the initial ring-opening step is reversible. DFT calculations indicated that the reverse reaction of the epoxide ring-opening has a very small barrier (6.5 kcal/mol for **2d**), supporting reversibility in the initial step.

(17) DFT calculations on the ring-opening reactions of **2d** with a single catalyst TBAX (TBAC, TBAB, and TBAI) were also carried out in the same way, and the optimized structures are given in the Supporting Information. The activation energies for TBAC, TBAB, and TBAI were calculated to be 22.3, 26.5, and 27.2 kcal/mol, respectively, predicting the relative catalytic activity as follows: TBAI < TBAB < TBAC. In fact, this agrees with the experimental results (Table 1). Therefore, the reversal of the nucleophilicity of the halide anion in **1** (Cl^- < Br^-) results from something specific to the bifunctional catalyst **1** as discussed in the main text and the Supporting Information. For the DFT calculations on similar systems, see: Wang, J.-Q.; Dong, K.; Cheng, W.-G.; Sun, J.; Zhang, S.-J. *Catal. Sci. Technol.* **2012**, *2*, 1480−1484.

(18) In the absence of the axial ligand, the Mg atom is located just inside the porphyrin cavity with an atomic charge of +1.43.

(19) The energy trough for intermediate **I2** may suggest the existence of a potential pathway to the formation of the alternating copolymer. However, even when a mixture of **2d** (0.29 g, 5.0 mmol), CO_2 (3.0 MPa), and **1d** (0.05 mol%) was stirred at ambient temperature (30 °C) for 24 h, **3d** was exclusively produced in 80% without any formation of polycarbonate. This result indicates that the structure of **1d** is highly tuned for the formation of cyclic carbonate.

(20) *CRC Handbook of Chemistry and Physics*, 75th ed.; Lide, D. R., Ed.; CRC: Boca Raton, FL, 1994.

(21) Judging from the poor coordinative abilities of **2** and **3** estimated from binding constants, we consider that product **3** on the catalyst can be easily replaced with substrate **2**. See the Supporting Information.

(22) Kubát, P.; Lang, K.; Anzenbacher, P., Jr.; Jursíková, K.; Král, V.; Ehrenberg, B. *J. Chem. Soc., Perkin Trans. 1* **2000**, 933−941.

(23) (a) Lee, C.; Yang, W.; Parr, R. G. *Phys. Rev. B* **1988**, *37*, 785−789. (b) Becke, A. D. *J. Chem. Phys.* **1993**, *98*, 5648−5652.

(24) (a) Hehre, W. J.; Ditchfield, R.; Pople, J. A. *J. Chem. Phys.* **1972**, *56*, 2257−2261. (b) Hariharan, P. C.; Pople, J. A. *Theor. Chim. Acta* **1973**, *28*, 213−222.

(25) (a) Miertuš, S.; Scrocco, E.; Tomasi, J. *Chem. Phys.* **1981**, *55*, 117−129. (b) Mennucci, B.; Tomasi, J. *J. Chem. Phys.* **1997**, *106*, 5151−5158. (c) Cammi, R.; Mennucci, B.; Tomasi, J. *J. Phys. Chem. A* **2000**, *104*, 5631−5637.

(26) We confirmed that the polarity of the solvent had only a small impact on the energy profile. See the Supporting Information.

(27) (a) Reed, A. E.; Weinhold, F. *J. Chem. Phys.* **1983**, *78*, 4066−4073. (b) Reed, A. E.; Weinstock, R. B.; Weinhold, F. *J. Chem. Phys.* **1985**, *83*, 735−746.

(28) Frisch, M. J.; et al. *Gaussian 09*, Revision B.1; Gaussian, Inc.: Wallingford, CT, 2009.